Developmental Cell
Article

Control of Hematopoietic Stem Cell Emergence by Antagonistic Functions of Ribosomal Protein Paralogs

Yong Zhang,[1,2] Anne-Cécile E. Duc,[1,2] Shuyun Rao,[1] Xiao-Li Sun,[1] Alison N. Bilbee,[1] Michele Rhodes,[1] Qin Li,[1] Dietmar J. Kappes,[1] Jennifer Rhodes,[1,2] and David L. Wiest[1,2,*]
[1]Blood Cell Development and Cancer Keystone, Immune Cell Development and Host Defense Program, Fox Chase Cancer Center, Philadelphia, PA 19111, USA
[2]These authors contributed equally to this work
*Correspondence: david.wiest@fccc.edu
http://dx.doi.org/10.1016/j.devcel.2013.01.018

SUMMARY

It remains controversial whether the highly homologous ribosomal protein (RP) paralogs found in lower eukaryotes have distinct functions and this has not been explored in vertebrates. Here we demonstrate that despite ubiquitous expression, the RP paralogs, Rpl22 and Rpl22-like1 (Rpl22l1) play essential, distinct, and antagonistic roles in hematopoietic development. Knockdown of Rpl22 in zebrafish embryos selectively blocks the development of T lineage progenitors after they have seeded the thymus. In contrast, knockdown of the Rpl22 paralog, Rpl22l1, impairs the emergence of hematopoietic stem cells (HSC) in the aorta-gonad-mesonephros by abrogating Smad1 expression and the consequent induction of essential transcriptional regulator, Runx1. Indeed, despite the ability of both paralogs to bind *smad1* RNA, Rpl22 and Rpl22l1 have opposing effects on Smad1 expression. Accordingly, circumstances that tip the balance of these paralogs in favor of Rpl22 (e.g., Rpl22l1 knockdown or Rpl22 overexpression) result in repression of Smad1 and blockade of HSC emergence.

INTRODUCTION

Ribosomal proteins (RP) are critical structural components of the ribosome that are usually essential for life (Amsterdam et al., 2004). Even mono-allelic inactivation of some RP has been implicated in human diseases, including *RPS14* in 5q- syndrome (Ebert et al., 2008) and *RPS19* in Diamond-Blackfan anemia (Draptchinskaia et al., 1999). These and other ribosomopathies share defects in hematopoiesis and in many cases an elevated risk of developing hematologic malignancies (Narla and Ebert, 2010). While the molecular basis for the tissue restriction of the phenotypes of ribosomopathies remains unclear, the common feature of hematopoietic defects reveal critical roles of these RP in blood cell development and transformation.

Mutations in individual RP are also reported to cause distinct and tissue-restricted developmental abnormalities in model organisms (Kondrashov et al., 2011). The distinct phenotypes have been proposed to result from individual RP performing differing functions from within "specialized ribosomes" or, alternatively, through "extraribosomal functions" outside of the ribosome, that influence cell growth, senescence, apoptosis, DNA repair, transcription, mRNA processing, and translation (Sonenberg and Hinnebusch, 2009; Warner and McIntosh, 2009; Xue and Barna, 2012). Among the best-characterized extraribosomal functions is regulation of p53 activation (Deisenroth and Zhang, 2010; Zhang and Lu, 2009). Disruption of ribosome biogenesis activates p53 by inducing nucleolar stress, which releases Rpl5, Rpl11, and Rpl23 from the nucleolus, and enables them to bind MDM2 and block MDM2-mediated p53 degradation (Deisenroth and Zhang, 2010; Pestov et al., 2001; Zhang and Lu, 2009). Another well established, extraribosomal function is the translational regulation of mRNAs bearing GAIT elements by Rpl13a (Mukhopadhyay et al., 2008).

Gaining insight into the critical functions of RP in lower organisms has been complicated by highly homologous RP paralogs (59 of 78 RP in *Saccharomyces cerevisiae* have paralogs). Loss-of-function analysis focused on growth defects in yeast revealed that most RP paralogs in yeast were able to cross-complement and were likely to be functionally redundant (Rotenberg et al., 1988). However, more recent analysis indicates that some RP paralogs may have unique functions (Haarer et al., 2007; Steffen et al., 2008). Analysis of the Rpl23aA/Rpl23aB paralogous pair in *Arabidopsis* revealed that while loss of Rpl23aA severely disrupted development, knockdown of Rpl23aB had no phenotype (Degenhardt and Bonham-Smith, 2008). Moreover, *rpl22a*Δ, but not *rpl22b*Δ, mutants exhibit a defect in bud site selection, which is not rescued by high copy number suppression with RPL22B (Komili et al., 2007). While the basis for these seemingly distinct functions remains unclear, these data support the notion that some RP paralogs can perform distinct functions.

The mammalian orthologs of yeast RPL22A and RPL22B are Rpl22 and Rpl22-like1 (Rpl22l1), respectively. Rpl22 is an RNA-binding protein component of the 60S ribosomal subunit that is dispensable for global protein synthesis, but can bind cellular and viral RNA, including telomerase RNA and Epstein-Barr Virus (EBV) EBER-1 RNA (Houmani et al., 2009). We have recently shown that despite ubiquitous expression, germline ablation of *Rpl22* causes an exquisitely selective defect in the development of αβ T lymphocytes (Anderson et al., 2007). The arrest is p53-dependent and results from translational de-repression of p53, rather than through the increased p53 stability that typically

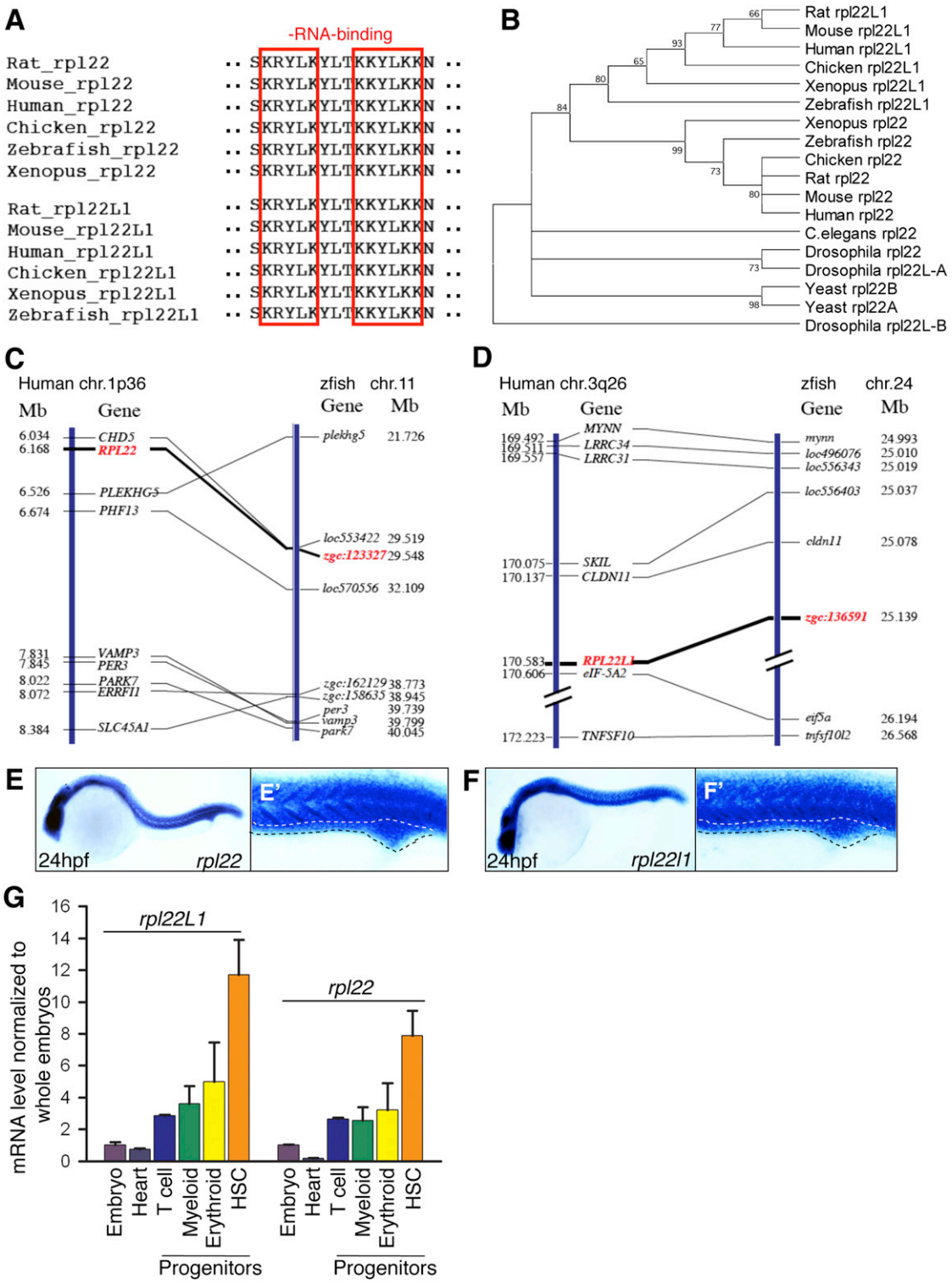

Figure 1. Bioinformatic and Expression Analysis of Zebrafish *rpl22* and *rpl22l1*

(A–D) Sequence alignment of RNA-binding domains, phylogenetic analysis, and synteny analysis. (A) Red-boxed area denotes RNA-binding motif. (B) Numbers on the branches of the phylogenetic tree are bootstrap values. (C) The human (1p36) and zebrafish *rpl22* (LG11) loci are flanked by a common set of genes (*CHD5*, *PLEKGH5*, *PHF13*, *VAMP3*, *PER3*, *PARK7*, *ERRF11*, and *SLC45A1*). (D) Human (3q26) and zebrafish *rpl22l1* (*lg24*) loci are flanked by a common set of genes (*MYNN*, *LRRC34*, *LRRC31*, *SKIL*, *CLDN11*, *EIF-5A2*, and *TNFSF10*). Orthologous *RPL22* and *RPL22L1* gene symbols are in red and bold.

(E–F′) Zebrafish *rpl22* and *rpl22l1* WISH analysis on 24 hpf embryos. (E and F) Lateral views with head to the left. (E′ and F′) Insets depict the ICM region delimited by dashed lines.

(legend continued on next page)

accompanies perturbed ribosome biogenesis (Anderson et al., 2007). Because p53 de-repression and developmental arrest are restricted to αβ T cells, we hypothesized that this might reflect compensation by the highly homologous paralog of Rpl22, RpL22l1 (Anderson et al., 2007). However, the function of RpL22l1 and its relationship to that of Rpl22 have not been explored in metazoans.

To address the function of Rpl22l1 in vertebrate development and its relationship to Rpl22, we utilized the zebrafish model (Goessling et al., 2007; Lieschke and Trede, 2009). We determined that the zebrafish orthologs of the mammalian *Rpl22* and *Rpl22l1* genes were widely expressed, but were enriched in hematopoietic stem and progenitor cells. Loss-of-function analysis revealed that these paralogs perform critical, tissue-restricted, distinct functions in hematopoiesis. Indeed, morpholino (MO) knockdown of Rpl22 caused a p53-dependent arrest in development of T cell progenitors after they have seeded the thymus. Conversely, knockdown of Rpl22l1 disrupted hematopoiesis in a distinct manner, by blocking the generation of Runx1-expressing, definitive hematopoietic stem cells (HSC) in the aorta gonad mesonephros (AGM) region. Importantly, the blockade of HSC emergence resulted from posttranscriptional repression of Smad1, which is controlled through the balance of the antagonistic actions of Rpl22 and Rpl22l1.

RESULTS

Identification of Zebrafish Orthologs of Rpl22 and Rpl22l1

The zebrafish orthologs of human Rpl22 (*zgc:123327*) and Rpl22l1 (*zgc:136591*) were identified by homology. Rpl22 and Rpl22l1 are highly conserved from human to zebrafish, are 73% identical (Figure S1A available online), and share identical RNA-binding motifs (Figure 1A, red boxes), but their sequences diverge at the amino (N) and carboxy (C) termini (Figure S1A). Phylogenetic tree analysis revealed that the zebrafish *rpl22* and *rpl221* genes are closely related to their mammalian orthologs (Figure 1B). Finally, *zgc:123327* and *zgc:136591* are syntenic to the human *RPL22* (1p36) and *RPL22L1* (3q26) loci, respectively (Figures 1C and 1D).

Whole mount in situ hybridization (WISH) revealed that zebrafish *rpl22* and *rpl22l1* are expressed both maternally and zygotically throughout early development (Figures S1B and S1C). Moreover, both were incorporated into ribosomes and polysomes engaged in translation (Figure S1D). *rpl22* and *rpl22l1* were also ubiquitously expressed at 24 hr postfertilization (hpf) (Figures 1E and 1F), including in the intermediate cell mass (ICM), a site of primitive hematopoiesis (Figures 1E′ and 1F′, ICM, dotted line). Quantification of *rpl22* and *rpl22l1* mRNA levels by real-time PCR revealed that expression of both *rpl22* and *rpl22l1* was markedly enriched in HSC, with *rpl22l1* expression being somewhat higher than *rpl22* (Figure 1G). Their expression in T lymphoid, erythroid, and myeloid progenitors was lower than in HSC, but still enriched relative to that in the embryo as a whole or in heart (Figure 1G). Thus, while Rpl22 and Rpl22l1 are widely expressed in zebrafish, they are enriched in hematopoietic tissues.

Rpl22l1 Knockdown Arrests T Cell Development in a p53-Dependent Manner

We reported previously that germline ablation of the widely expressed *Rpl22* gene in mouse caused a highly-selective, p53-dependent arrest in αβ-lineage T cell development (Anderson et al., 2007). To determine if that was true for loss of Rpl22 and Rpl22l1 in zebrafish, we knocked down their expression and assessed the effect on development of T cells marked by an *lck:EGFP* transgene (Langenau et al., 2004). To do so, we employed a translational start site antisense MO for Rpl22 and a splice-site MO for Rpl22l1, both of which effectively reduced expression from 1 dpf to 5 dpf (Figures S2A–S2F). Neither *rpl22* morpholino-injected (morphant) nor *rpl22l1* morphant embryos exhibited gross developmental defects through 5 dpf (Figures S2G and S2H). Importantly, the morpholinos employed were specific, as neither reduced expression of the cognate paralog (Figures S2I and S2J). Surprisingly, both *rpl22* and *rpl22l1* morphants lacked GFP^+ cells in the thymus, indicating a block in T cell development and suggesting that each RP played a distinct, but essential role in T cell development (Figures 2A and 2C). As was true in Rpl22-deficient mice, the block in T cell development in *rpl22* morphants was associated with increased apoptosis as indicated by TUNEL staining, and was rescued by p53-deficiency (Figures 2A′, 2B, and 2B′) (Anderson et al., 2007). While disruption of ribosome biogenesis can trigger nucleolar stress and activate p53-dependent apoptosis, our analysis of Rpl22-deficient mice suggested that Rpl22-deficiency was not activating p53 by impairing ribosome biogenesis, since neither rRNA processing nor the polysome profile was altered (Anderson et al., 2007; Deisenroth and Zhang, 2010) (data not shown). The absence of an effect on ribosome biogenesis presumably explains why *rpl22* morphants do not exhibit the kind of gross morphologic defects associated with knockdown of other RP (Anderson et al., 2007; Chakraborty et al., 2009; Danilova et al., 2008). Like the *rpl22* morphants, *rpl22l1* morphants also exhibited a block in T cell development (Figure 2C), but it was not associated with increased apoptosis, nor was it rescued by p53-deficiency (Figures 2C–2D′). Thus, both Rpl22 and its paralog, Rpl22l1, play essential roles in T cell development; however, they differ in induction of apoptosis and p53-dependence, suggesting that they perform distinct functions.

The Functions of Rpl22 and Rpl22l1 Are Critical in Distinct Progenitor Pools

To gain insight into the T cell progenitor populations that might be differentially dependent upon Rpl22 and Rpl22l1, we

(G) Real-time PCR quantification of *rpl22* and *rpl22l1* mRNA levels in hematopoietic progenitor populations. Tg fish lines were employed to identify the following progenitors: (1) heart, *cmcl2:EGFP* at 2 dpf, (2) T cell, *lck:EGFP* at 5 dpf, (3) myeloid, *mpo:EGFP* at 5 dpf, (4) erythroid, *gata1:dsRED2* at 5 dpf, and (5) HSC, *cd41:EFGP* at 3.5 dpf. GFP+ cells were isolated by flow cytometry, after which *rpl22* and *rpl22l1* expression was measured by real-time PCR. Results of triplicate measurements were normalized to *b-actin* and whole embryo homogenates and represented graphically as the mean ± SD.

The results were combined from at least three separate experiments with representative photographs depicting the observed phenotypes. Unless otherwise specified, all images represent lateral views with the head to the left. See also Figure S1.

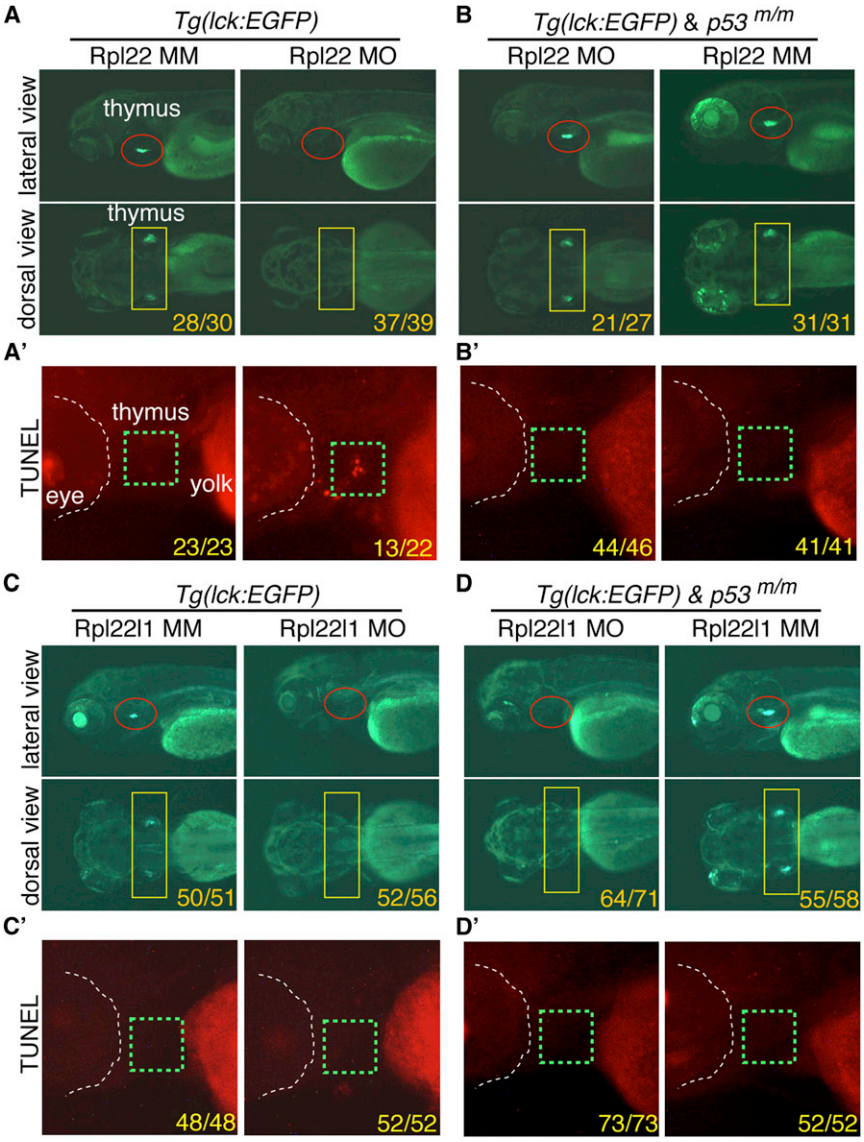

Figure 2. The Arrest of Thymocyte Development in *rpl22*, but Not *rpl22l1*, Morphants Is p53-Dependent

(A–D′) Knockdown of both Rpl22 and Rpl22l1 arrest T cell development, but the arrest in *rpl22l1* morphants is p53-independent. Rpl22 and Rpl22l1 were knocked down in p53-sufficient (A and C) or p53-deficient (*p53m/m*; B and D) *Tg(lck:EGFP)* embryos by injection of 1 ng of Rpl22 MO, Rpl22l1 MO, or MM control, after which T cell development was assessed microscopically by scoring for the loss of GFP-marked T cell progenitors at 5 dpf (lateral view, red circles; dorsal view, yellow rectangles). Effects on apoptosis in the thymus (green dashed rectangles) were assessed at 3.5 dpf by TUNEL staining (A′, B′, C′, and D′).

Images depict phenotypes representative of at least three separate experiments, with numbers referring to the fraction of morphants with the depicted phenotypes. See also Figure S2.

performed WISH on morphants at 5 dpf using probes identifying important regulators of T cell development (Figure 3). These probes include: (1) *foxn1*, a transcription factor required for generation of thymic epithelium (Su et al., 2003), (2) *ikaros*, a DNA-binding protein required for lymphoid development (Georgopoulos et al., 1997), (3) *rag1*, a lymphocyte-specific nuclease required for T cell antigen receptor (TCR) gene rearrangement, (4) *lck*, a tyrosine kinase required for T cell development (Langenau et al., 2004), and (5) TCRβ (*tcrb*) and TCRδ (*tcrd*) subunits that identify αβ-lineage and γδ-lineage progenitors, respectively (Lee et al., 2010). WISH using probes marking T lineage progenitors (Figure 3A; *ikaros*, *rag1*) revealed that knockdown of Rpl22 did not impair seeding of the thymus; however, it did impair progenitor development and expansion as indicated by the reduced staining with probes that mark more mature progeny (Figure 3A; *lck*, *tcrb*). The block in T cell development in *rpl22* morphants was selective for αβ T cells, since γδ progenitors were unaffected (Figure 3A; *tcrd*), as we observed previously in Rpl22-deficient mice (Anderson et al., 2007). In contrast, WISH analysis of the *rpl22l1* morphants revealed that staining with all of the probes described above was dramatically reduced (Figure 3B). This suggested that unlike Rpl22, whose elimination selectively blocked αβ T cell development after thymus seeding, knockdown of Rpl22l1 blocked development of both αβ and γδ T cells, possibly by preventing thymus seeding. The absence of thymic progenitors in *rpl22l1* morphants was not due to a perturbation of the vasculature or thymic stroma, since these structures were unchanged (Figures S3A and S3B). Thus, these data suggest that the arrest of T cell development in *rpl22* and *rpl22l1* morphants results from effects on distinct progenitor populations.

Rpl22l1 Is Required for HSC Emergence and Thymic Seeding

The loss of intrathymic progenitors in *rpl22l1* morphants suggested that either their generation or their seeding was disrupted. T cell development begins at 2 dpf when the thymic rudiment is seeded by CD41+ progenitors, which derive from the CD41+Runx1+ definitive HSC that emerge from the ventral wall of the dorsal aorta (VDA) between 24 and 30 hpf (Boehm and Bleul, 2006; Jin et al., 2007; Lam et al., 2009). To investigate whether loss of Rpl22l1 interferes with thymic seeding, we knocked Rpl22l1 down in *Tg(cd41:EGFP)* reporter fish and determined if the accumulation of CD41+ progenitors in the thymus was impaired (Bertrand et al., 2008; Kissa et al., 2008). Indeed, loss of Rpl22l1 blocked the appearance of CD41-EGFP^{low} progenitors in the thymus at 3.5 dpf and 5 dpf (Figures 3C and

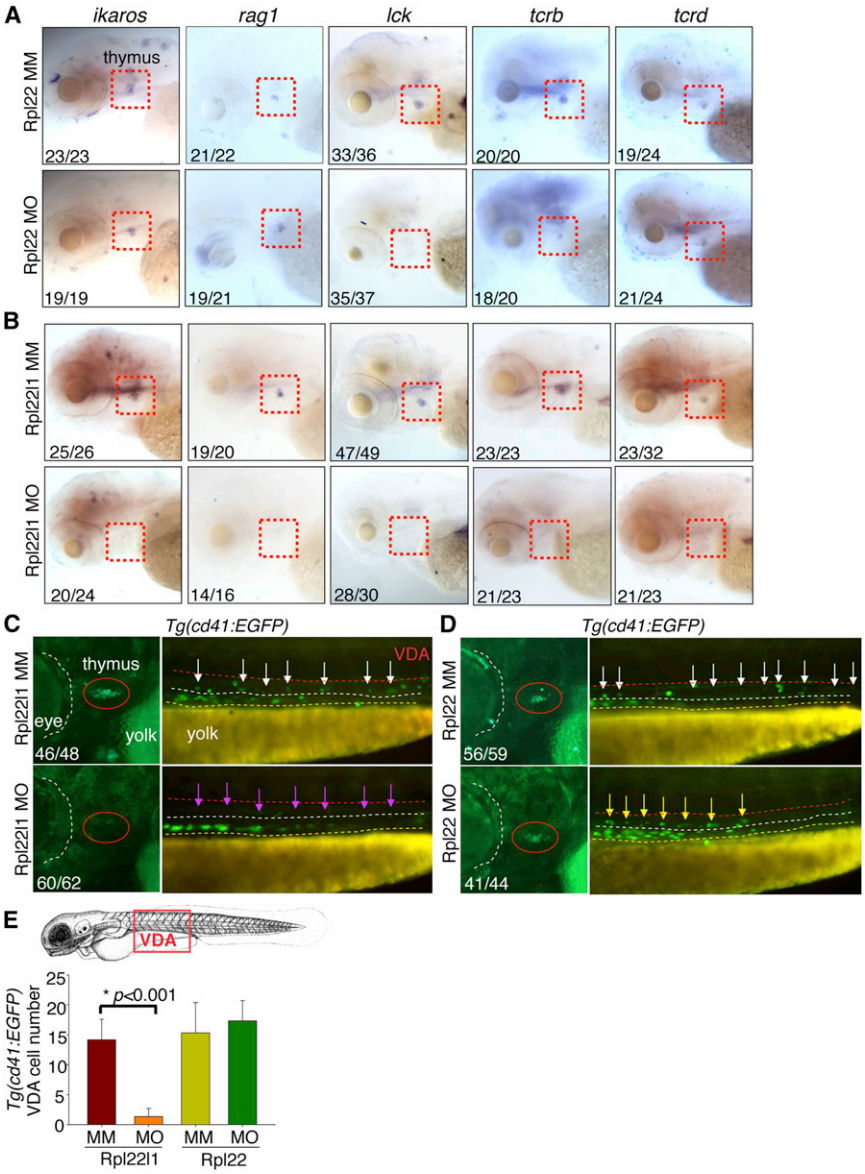

Figure 3. Distinct, Lineage-Restricted Defects in Hematopoiesis in *rpl22* and *rpl22l1* Morphants

(A and B) WISH analysis of thymocyte development with the indicated probes in *rpl22* (A) and *rpl22l1* morphants (B) at 5 dpf. Thymus, red dashed rectangles.

(C–E) Evaluation of thymus colonization and HSC emergence in *rpl22l1* and *rpl22* morphants. *Tg(cd41:EGFP)* embryos were injected with Rpl22l1 MO, Rpl22 MO, or MM control, after which seeding of the thymus and HSC emergence was assessed at 3.5 dpf by tracking the presence of GFP+ cells in the thymus (red circles) or VDA (between the red and white dashed lines). Emerging HSC are indicated by arrows. The area between the dashed white and yellow lines is the pronephric duct. The number of CD41-EGFP^{low} HSCs was quantified in six representative embryos per group and presented as mean ± SD. *$p < 0.001$.

Images depict phenotypes representative of at least three separate experiments, with numbers referring to the fraction of morphants with the depicted phenotypes. See also Figure S3.

S3C, red oval). The absence of CD41-EGFP^{low} progenitors in the thymus resulted from impaired HSC generation in the VDA, since CD41-EGFP^{low} HSCs were reduced in *rpl22l1* morphants relative to control-treated embryos (Figures 3C, purple arrows, and 3E). The reduction in CD41-EGFP marked cells was restricted to HSC, as nonhematopoietic CD41-EGFP^{+} cells in the pronephric tubules were not affected by Rpl22l1 knockdown (Figure 3C, between yellow and white dashed lines). Identical results were obtained using a second *rpl22l1* morpholino that blocks Rpl22l1 translation (Figures S3E–S3H). CD41-EGFP^{High} thrombocytes in the caudal hematopoietic tissue (CHT) were also markedly reduced by Rpl22l1 knockdown, an expected consequence of impairing the generation of HSC from which they derive (Figure S3C, purple arrowheads). In striking contrast, knockdown of Rpl22 did not cause any alterations in accumulation of CD41-marked progenitor cells in the thymus, VDA, or CHT (Figures 3D, 3E, and S3D), confirming that T progenitors in *rpl22* morphants were able to seed the thymus, but failed to develop further. The impairment of HSC emergence by Rpl22l1 knockdown, also inhibited the development of definitive progenitors that arise from HSC. These included definitive erythroid progenitors, which were reduced in both CHT and kidney, where hematopoiesis occurs in the adult (Jin et al., 2007) (Figure 4A; *ae1-globin*), as well as, *lyc*+ definitive myeloid progenitors, which were reduced in the VDA and kidney at 5 dpf (Figure 4B). Thus, knockdown of Rpl22l1 and Rpl22 blocks T cell development by acting on different progenitor populations. Rpl22 knockdown blocks development of progenitors after thymic seeding. In contrast, Rpl22l1 knockdown blocks T cell development by preventing the generation of definitive HSC and their downstream progeny, including those of the T, erythroid, and myeloid lineages.

Rpl22l1 Knockdown Blocks Production of Runx1+ Progenitors

Having demonstrated that Rpl22l1 loss impaired the emergence of definitive HSC, we sought to understand the basis for this block by investigating the expression of transcriptional regulators of HSC specification (Lam et al., 2010). We found that expression of c-*myb*, a marker of definitive HSC, was strikingly reduced in *rpl22l1* morphants at 5 dpf in the thymus (Figure 4C, red circle), as well as in the kidney (Figure 4C, blue asterisk) (Jin et al., 2007; Murayama et al., 2006). *myb* expression was also reduced in *rpl22l1* morphants in the AGM at 36 hpf, suggesting that Rpl22l1 is required for the initiation

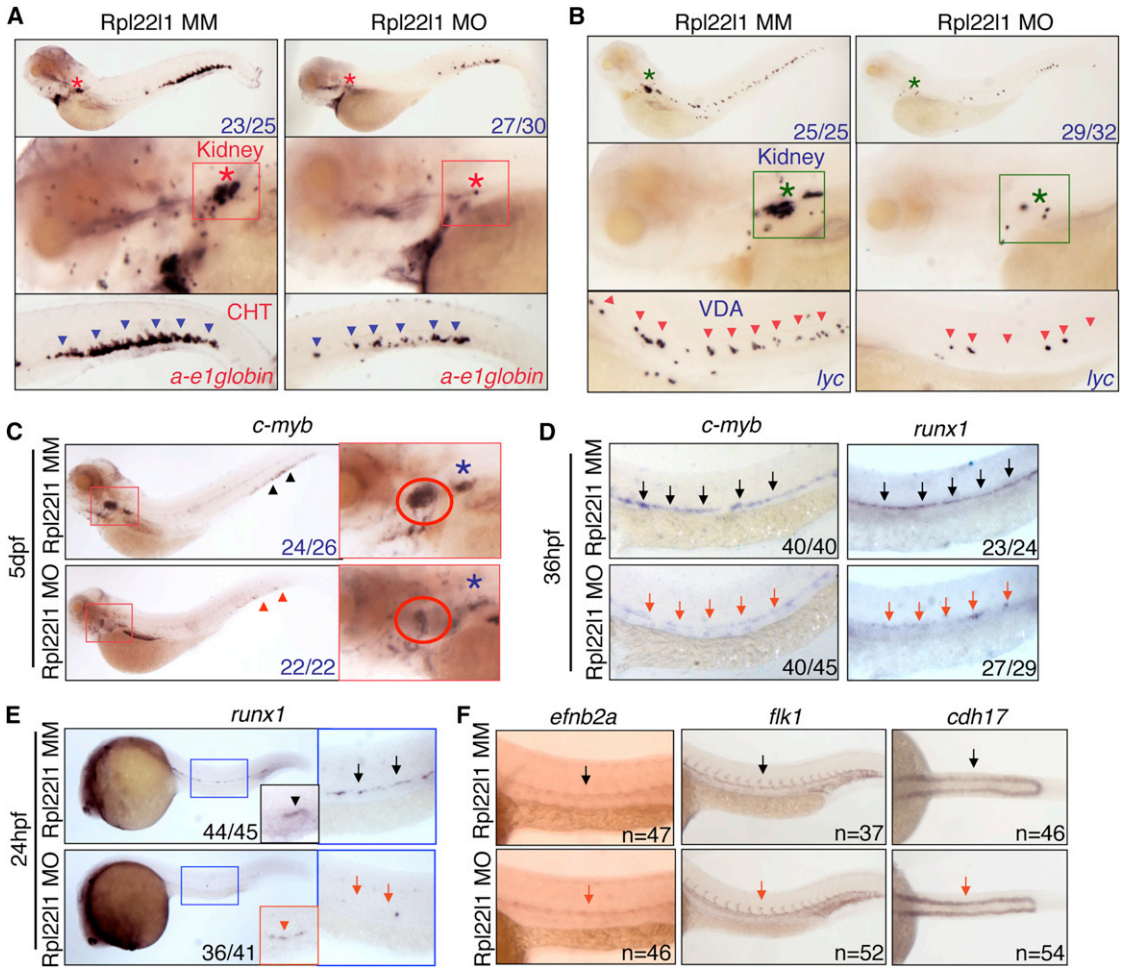

Figure 4. Rpl22l1 Knockdown Blocks HSC Emergence and Definitive Hematopoiesis

(A and B) The effect of Rpl22l1 knockdown on development of definitive erythroid (A; *a-e1globin*) and myeloid (B; *lyc*) progenitors was assessed by WISH with the indicated probes at 5 dpf in embryos injected with Rpl22l1 MO or MM control. Developing kidney, boxed area and asterisk; CHT, blue arrowheads; VDA, red arrowheads.

(C–E) Effect of Rpl22l1 knockdown on *c-myb* and *runx1* expressing progenitors. Embryos were injected with MO as above and evaluated by WISH at 5 dpf (C), 36 hpf (D), and 24 hpf (E) with the indicated probes. Developing kidney (C; red boxed insert, blue asterisk); thymus (C; red boxed inset, red circle); AGM, (D; arrows); AGM (E; blue boxed area, arrows); and erythro-myeloid progenitors (E; EMP, red boxed inset, red arrowhead).

(F) Impact of Rpl22l1 knockdown on the vasculature. Dorsal aorta (*efnb2a*), vasculature (*flk1*), and pronephros (*cdh17*) were assessed by WISH in control and *rpl22l1* morphant embryos as above with the indicated probes (arrows).

Images depict phenotypes representative of at least three separate experiments, with numbers referring to the fraction of morphants with the depicted phenotypes. See also Figure S4.

and/or maintenance of definitive hematopoiesis (Figure 4D). The blockade in emergence of CD41+ *myb*-expressing progenitors in *rpl22l1* morphants closely resembles the phenotype resulting from Runx1 knockdown (Kissa and Herbomel, 2010; Kissa et al., 2008; Wilkinson et al., 2009). Because Runx1 is essential for HSC emergence in both mouse and zebrafish (Bertrand et al., 2010, 2008; Boisset et al., 2010; Chen et al., 2009; Kissa and Herbomel, 2010; Lam et al., 2010), and because its expression is one of the earliest markers of HSC emergence (Bajoghli et al., 2004; Lam et al., 2010), we asked if Rpl22l1 knockdown interfered with *runx1* expression in the AGM. Indeed, *rpl22l1* morphants exhibited reduced expression of *runx1* in the VDA at both 24 hpf and 36 hpf (Figures 4D and 4E, large inset). The reduced *runx1* expression did not result from impaired specification of the dorsal aorta, since WISH analysis using *efnb2a*, a marker for dorsal aorta, revealed that it was unaffected in *rpl22l1* morphants (Figure 4F). *rpl22l1* morphants also had normal vasculature (Figure 4F, *flk1*) and pronephros (Figure 4F, *cdh17*). Interestingly, the attenuation of *runx1* expression in *rpl22l1* morphants was selective for definitive HSC, as *runx1* expression in primitive erythro-myeloid progenitors in the PBI was not as severely affected (Figure 4E, arrowheads and small insets). Likewise, other markers of primitive hematopoiesis were also unaffected in *rpl22l1* morphants at 24 hpf (Figures S4A and S4B), and in some cases were actually increased (Figures S4C–S4E; e.g., *gata1*, primitive erythroid progenitors).

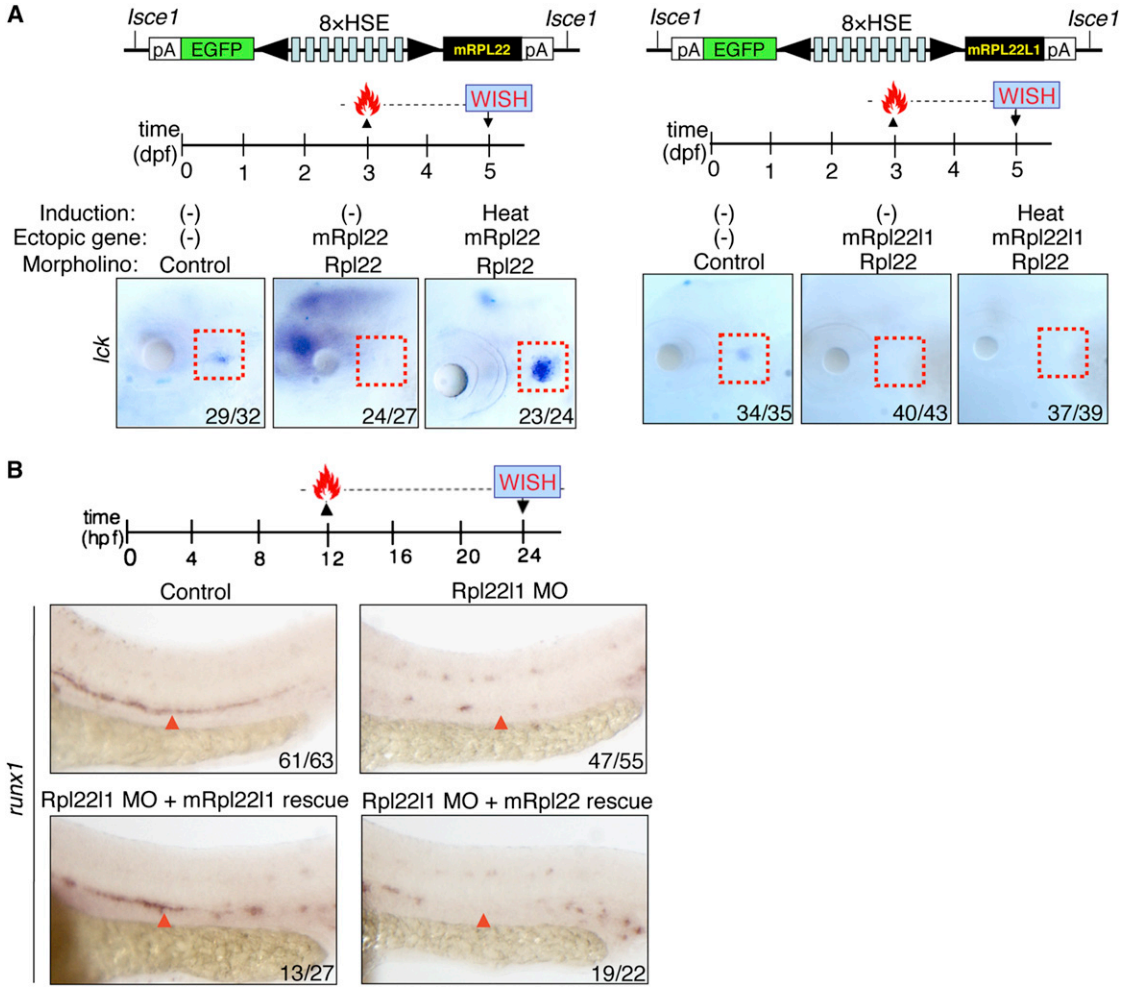

Figure 5. Rpl22 and Rpl22l1 Are Unable to Cross-Compensate Defects Caused by Loss of Their Paralog

(A and B) Cross-complementation analysis of the hematopoietic defects caused by knockdown of Rpl22 and Rpl22l1. Embryos injected with Rpl22 MO, Rpl22l1 MO, or MM control were coinjected with the indicated heat-inducible rescue plasmids. Expression of Rpl22/Rpl22l1 was restored by heating for 1 hr at 37°C at either 3 dpf (A) or 12 hpf (B) after which effects on T cell development were assessed by WISH at 5 dpf with an *lck* probe (A) and effects on HSC emergence were assessed at 24 hpf using a *runx1* probe. Thymocytes (A; red dashed rectangles). HSC (B; red arrowheads).

Images depict phenotypes representative of at least three separate experiments, with numbers referring to the fraction of morphants with the depicted phenotypes. See also Figures S5.

Thus, while Rpl22l1 is required for the emergence of *runx1*+ definitive HSC, it is dispensable for primitive hematopoiesis. In contrast, Rpl22 knockdown caused no perturbations in the aforementioned markers of stem cell emergence, vasculature, or primitive hematopoiesis (Figures S4F–S4H); however, *rpl22* morphants did exhibit a slight reduction in definitive erythroid progenitors and a modest increase in definitive myeloid progenitors (Figures S4I and S4J). Importantly, these observations provide further support that Rpl22 and Rpl22l1 are performing distinct functions in distinct progenitor pools. It should be noted that the blockade in development of *runx1*+ HSC in *rpl22l1* morphants is not p53-dependent, as there was no increase in apoptosis in the VDA, and the block was not rescued by inactivation of p53 (Figure S5), suggesting that Rpl22l1 loss is not impairing HSC specification in a p53-dependent manner.

Rpl22 and Rpl22l1 Are Unable to Reciprocally Rescue the Developmental Arrest Caused by Loss of Their Paralog

Rpl22 and Rpl22l1 knockdown might cause distinct developmental defects either because they perform distinct functions or because they exhibit different expression patterns. To distinguish these possibilities, we performed reciprocal rescue experiments in *rpl22* and *rpl22l1* morphants by enforcing the expression of MO-resistant forms of either Rpl22 or Rpl22l1 in a heat-inducible manner (Figures 5A, S5C, and S5D) (Bajoghli et al., 2004). To assess the respective abilities or Rpl22 and Rpl22l1 to circumvent the block in T cell development caused by Rpl22 knockdown, *rpl22* morphants were injected with heat-inducible expression constructs encoding morpholino-resistant murine Rpl22 and Rpl22l1, heat-induced at 3 dpf, and analyzed at 5 dpf (Figure 5A, red rectangles). WISH analysis on

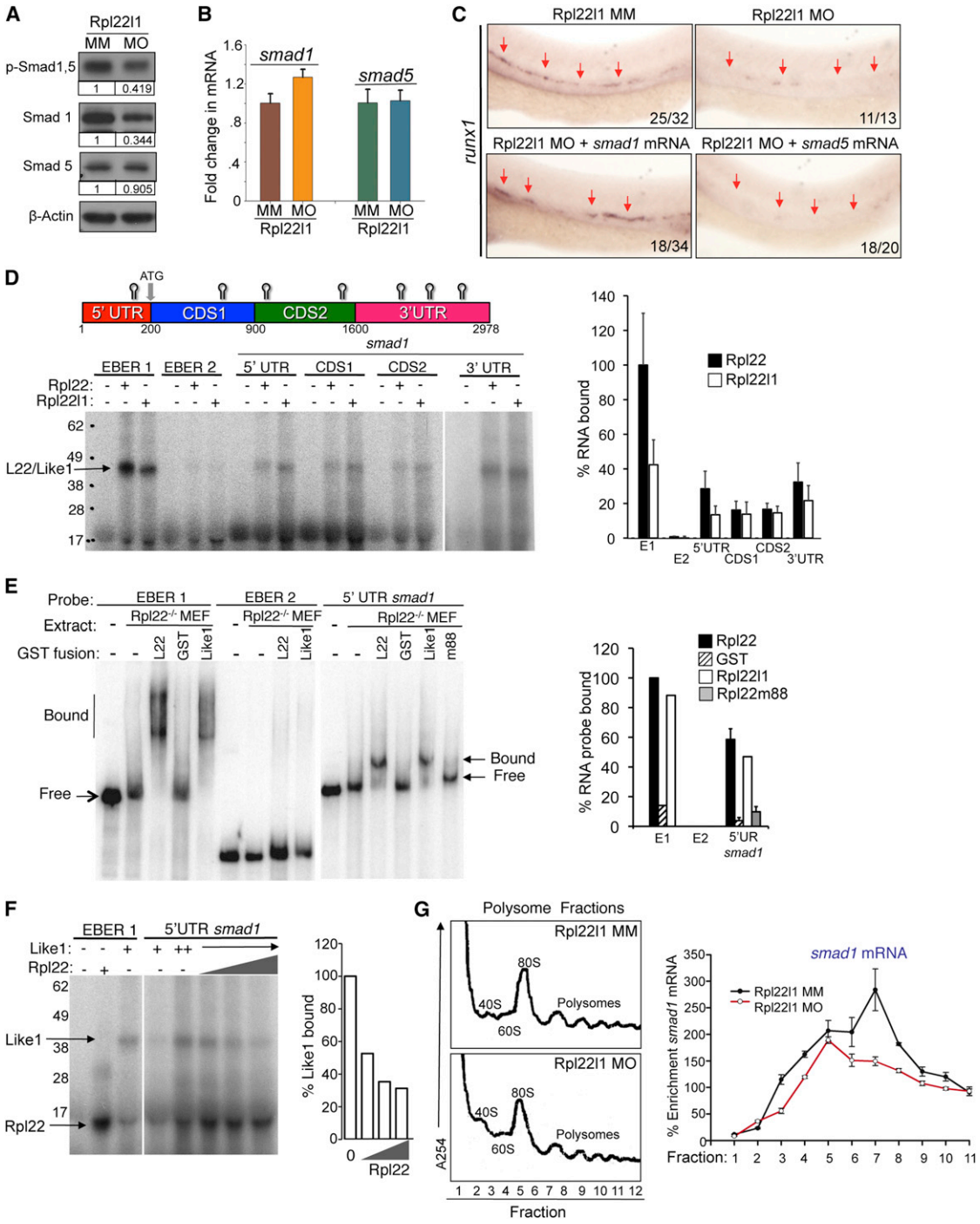

Figure 6. The Blockade of HSC Emergence in *rpl22l1* Morphants Results from Reduced Smad1 Expression

(A and B) Effect of Rpl22l1 knockdown on Smad expression. The expression levels and phosphorylation of Smad1 and Smad5 were measured by immunoblotting of controls and *rpl22l1* morphants at 24 hpf. β-actin was used as a loading control. Band intensity relative to control is indicated. (B) *smad1* and *smad5* mRNA levels were quantified by real-time PCR and normalized to *b-actin*, after which the mean ± SD was depicted graphically.

(C) Complementation of the arrest in HSC emergence in *rpl22l1* morphants by Smad1. The indicated mRNAs (100 pg) were injected in *rpl22l1* morphants after which the emergence of HSC was evaluated by WISH using a *runx1* probe. Images depict phenotypes representative of at least three separate experiments, with numbers referring to the fraction of morphants with the depicted phenotypes.

(D–F) Analysis of binding of *smad1* mRNA by Rpl22 and Rpl22l1. (D) Schematic depicting the location in *smad1* mRNA of Rpl22/Rpl22l1 binding sites predicted using M-Fold. The indicated radiolabeled mRNA probes were incubated with GST-hRpl22 (Rpl22) or GST-mRpl22l1 (Rpl22l1), after which binding was assessed by RPA. Binding was quantified by phosphorimagery, normalized to the level of Rpl22 binding to EBER1 (E1, positive control), and the mean ± SD depicted graphically (right). EBER2 (E2) served as a negative control. (E) Binding of Rpl22, Rpl22l1, and RNA-binding mutant Rpl22 (m88) to the 5′ UTR of *smad1* mRNA was

(legend continued on next page)

EGFP+ embryos using an *lck* probe revealed that enforced expression of Rpl22 rescued thymocyte development in *rpl22* morphants, in a heat-shock-inducible manner (Figure 5A, left); however, ectopic expression of Rpl22l1 failed to do so (Figure 5A, right). To assess the respective abilities or Rpl22 and Rpl22l1 to circumvent the block in HSC emergence caused by knockdown of Rpl22l1, *rpl22l1* morphants were injected with the same heat-inducible expression constructs, heat-induced at 12 hpf and analyzed by WISH at 24 hpf using *runx1* to mark emerging HSC (Figure 5B). Enforced expression of Rpl22l1 rescued HSC emergence in *rpl22l1* morphants; however, enforced expression of Rpl22 was unable to do so (Figure 5B, red arrowheads). Collectively, the inability of each RP to rescue the developmental arrest caused by loss of its cognate paralog, demonstrates that despite their high degree of sequence identity, Rpl22 and Rpl22l1 perform critical, tissue-restricted roles in hematopoiesis that are distinct from one another, with Rpl22 being essential for development of thymic progenitors after arrival in the thymus, and Rpl22l1 acting much earlier to regulate the emergence of HSC in the AGM.

Both Rpl22 and Rpl22l1 Bind *smad1* mRNA but Have Opposing Effects on Expression

In zebrafish, the BMP4, Notch, hedgehog, and VEGF signaling pathways are all important for HSC emergence from the VDA (Wilkinson et al., 2009). Among these pathways, BMP signaling induces hematopoietic mesoderm through the downstream transcription factors, Smad1, 5, and 8 (McReynolds et al., 2007; Wilkinson et al., 2009), which can transactivate the *runx1* promoter (Pimanda et al., 2007). Moreover, knockdown of either BMP4 or Smad1 blocks HSC emergence while sparing primitive hematopoiesis, just as we observe in *rpl22l1* morphants (Figures S4C–S4E) (McReynolds et al., 2007; Wilkinson et al., 2009). Accordingly, to determine if alterations in BMP signaling were responsible for the phenotype of *rpl22l1* morphants, we asked whether Smad1/5 phosphorylation was altered (Tucker et al., 2008). Indeed, both Smad1/5 phosphorylation and Smad1 expression were decreased (Figure 6A), strongly suggesting that BMP/Smad signaling was impaired. While Smad1 protein levels were decreased to approximately one-third of the control expression level at 24 hpf (Figure 6A), Smad1 mRNA levels were unchanged, indicating that the reduction in *smad1* protein was occurring posttranscriptionally (Figure 6B). To determine if the reduction in Smad1 expression was responsible for impairing HSC emergence in *rpl22l1* morphants, we attempted to rescue development by ectopic expression of Smad1 and Smad5. Indeed, injection of *smad1*, but not *smad5*, mRNA partially rescued *runx1* expression in the VDA of *rpl22l1* morphants (Figure 6C, arrows). Together, these data indicate that Rpl22l1 promotes the emergence of *runx1*+ HSC by supporting BMP signaling, through facilitating the expression of Smad1.

Rpl22 and Rpl22l1 have identical RNA-binding helices, but play distinct roles in hematopoiesis. Accordingly, we propose that these paralogs might do so by binding to a similar cohort of mRNA targets while having opposing effects on their expression, thereby functioning antagonistically in some contexts. Since Smad1 is critical for HSC emergence and its expression is reduced in *rpl22l1* morphants, we asked if the reduction of Smad1 in *rpl22l1* morphants results from repression by Rpl22. Previous analysis showed that Rpl22 binds the EBV latency RNA EBER1, and other targets, via a loosely defined stem-loop motif (Dobbelstein and Shenk, 1995). M-fold analysis predicted the presence of several Rpl22/Rpl22l1 binding sites in *smad1* mRNA (Figure 6D). To assess whether *smad1* mRNA could be bound by both Rpl22 and Rpl22l1, we performed RNase protection analysis (RPA). RPA revealed that both Rpl22 and Rpl22l1 bound not only EBER1, but also bound to multiple domains of *smad1* mRNA (Figure 6D). Rpl22 and Rpl22l1 binding to *smad1* mRNA was confirmed by electrophoretic mobility shift assay (EMSA), using extracts from *Rpl22*−/− mouse embryonic fibroblasts supplemented with recombinant Rpl22 or Rpl22l1 (Figure 6E). Indeed, both Rpl22 and Rpl22l1 were able to induce a quantitative shift in the *smad1* 5′UTR mRNA and that binding was abrogated by mutating the RNA-binding domain of Rpl22 (m88; Figure 6E). Our model that Rpl22 and Rpl22l1 can bind a similar set of RNAs but have distinct effects on their expression suggests that they may compete for binding to *smad1*. In agreement, Rpl22l1 binding to the 5′ UTR of *smad1* mRNA was partially displaced by increasing amounts of a smaller, His-tagged Rpl22 fusion protein (Figure 6F). Finally, if the posttranscriptional reduction of Smad1 expression in *rpl22l1* morphants results from decreased translation, then *smad1* mRNA in polysomes should be reduced. Sucrose gradient analysis of polysomal profiles of *rpl22l1* morphants revealed that while the polysome trace was not significantly altered, *smad1* mRNA was shifted away from the polysome fractions, consistent with a reduction in Smad1 translation (Figure 6G). Together, these observations support a model where both Rpl22 and Like1 bind *smad1* mRNA, but have antagonistic effects on Smad1 protein levels, with Rpl22 acting to repress expression and Rpl22l1 acting to oppose that repression.

To test this model, we assessed how overexpression of Rpl22 and Rpl22l1 affected Smad1 protein levels. Injection of *rpl22* mRNA into zebrafish embryos repressed endogenous Smad1 protein levels and blocked the generation of *runx1*+ HSC in the VDA at 24 hpf (Figures 7A and 7B). In contrast, injection of

assessed by EMSA in which detergent extracts of *Rpl22*−/− MEF were supplemented with the indicated fusion proteins. Positions of bound and free probes are marked. The fraction of bound probe was quantified by phosphorimagery and represented graphically as above. Results represent the mean ± SD of three experiments performed. (F) Rpl22 competes with Rpl22l1 for binding to the 5′UTR of *smad1* mRNA. RPA analysis was performed with GST-Rpl22l1 as in (D), except that a smaller His-tagged Rpl22 fusion protein was added in increasing amounts to determine if it could displace bound GST-Rpl22l1. The bands corresponding to GST-Rpl22l1 (Like1) and His-Rpl22 (Rpl22) are indicated. The fraction of Rpl22l1 bound to *smad1* RNA in the presence of increasing quantities of Rpl22 was quantified and depicted graphically as a fraction of that bound in the absence of Rpl22.

(G) Polysome analysis of *rpl22l1* morphants. Detergent extracts of 24hpf control (MM) or *rpl22l1* morphant embryos were fractionated by ultracentrifugation on a sucrose gradient. The position of monosomes and polysomes was identified by monitoring O.D.254. *smad1* RNA content of each fraction was quantified by real-time PCR and normalized to *gapdh* as well as the level in unfractionated extract, which was defined as 100%. The mean of triplicate samples ± SD is depicted graphically on the right.

All results of representative of at least three experiments performed.

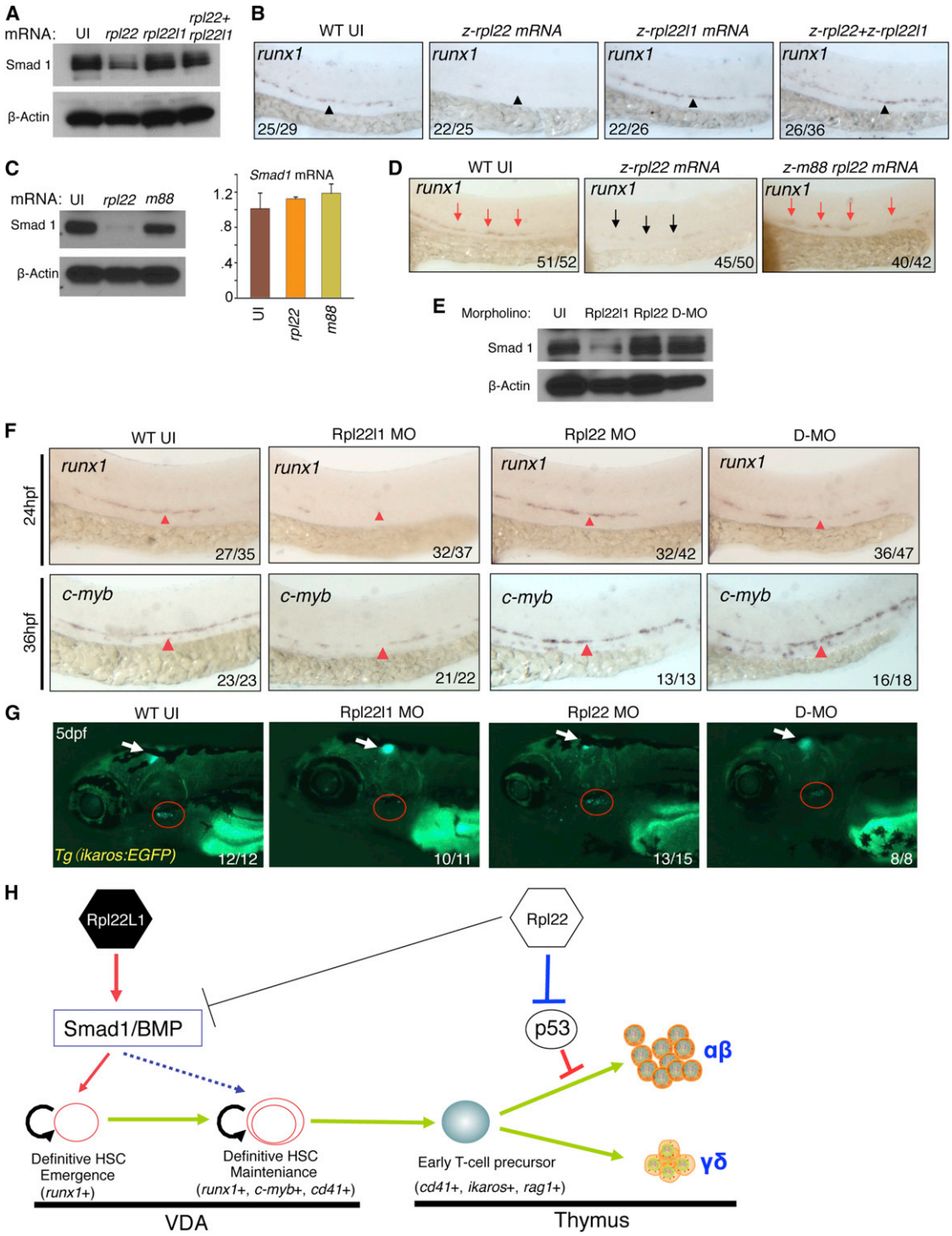

Figure 7. Opposing Roles of Rpl22 and Rpl22l1 in Regulating Smad1 Expression and HSC Emergence

(A and B) Effect of Rpl22 and Rpl22l1 overexpression on Smad1 protein levels and HSC emergence. RNA (100 pg) encoding *rpl22*, *rpl22l1*, or both were injected into embryos and the effect on Smad1 protein levels assessed by western blotting at 24 hpf (A). β-actin served as a loading control. The effect on HSC emergence in the AGM was assessed by WISH for *runx1* at 24 hpf (B).

(C and D) Requirement of Rpl22 RNA binding ability in regulating Smad1 expression and HSC emergence. mRNA encoding intact (75 pg) or RNA binding mutant *rpl22* (m88) (75 pg) was injected into embryos and the effect on Smad1 protein levels was assessed by blotting at 24 hpf, as above. The effect on *smad1* mRNA levels was determined using real-time PCR and the mean ± SD was depicted graphically (C). The effect on HSC emergence was assessed by WISH as above (D).

(E–G) Rescue of developmental arrest in *rpl22l1* morphants by knockdown of Rpl22. MO targeting Rpl22 (1 ng), Rpl22l1 (1 ng), or the two together (D-MO) were injected into zebrafish embryos, after which Smad1 protein expression was assessed at 24 hpf as above (E). The effect on HSC emergence was assessed by

(legend continued on next page)

rpl22l1 mRNA did not suppress Smad1 expression or impair HSC emergence. Importantly, however, coinjection of both *rpl22l1* and *rpl22* mRNA antagonized the ability of Rpl22 to repress Smad1, and rescued the emergence of *runx1*+ HSC (Figures 7A and 7B). The ability of Rpl22 to repress Smad1 was dependent upon its ability to bind RNA (Figures 7C and 7D; m88). Finally, as shown earlier, knockdown of Rpl22l1, but not Rpl22, reduced Smad1 protein expression and impaired the generation of *runx1*+ and c-*myb*+ HSC in the VDA, respectively (Figures 7E and 7F). This was also observed upon knockdown of Rpl22l1 using a second, translational start site morpholino (Figures S6A and S6B). Our antagonism model posits that Rpl22l1 knockdown reduces Smad1 levels because there is no Rpl22l1 to oppose Smad1 repression by Rpl22. Accordingly, Smad1 expression and HSC emergence should be restored in *rpl22l1* morphants by knockdown of Rpl22. Indeed, in double morphants (*rpl22l1* and *rpl22*), we found that Smad1 protein expression was restored to that observed in untreated embryos (Figure 7E; D-MO). Moreover, simultaneous knockdown of both Rpl22 and Rpl22l1 not only restored the development of *runx1*+ and c-*myb*+ HSC in the VDA at 24 and 36 hpf, respectively, but also restored thymic seeding by *Tg(lkaros-EGFP)* marked progenitors at 5 dpf (Figures 7F and 7G). Importantly, knockdown of Rpl22 and Rpl22l1 in double morphants was as effective as in single morphants (Figure S6C). Taken together, these data demonstrate that Rpl22 and Rpl22l1 regulate HSC emergence through antagonistic effects on Smad1 expression.

DISCUSSION

We report here that despite their high sequence homology, Rpl22 and its paralog Rpl22l1 perform critical, distinct, tissue-restricted roles in hematopoiesis (Figure 7H). Indeed, while both Rpl22 and Rpl22l1 are essential for T lymphocyte development, they support this process through distinct mechanisms, operating in distinct progenitor pools. Rpl22 is dispensable for HSC emergence and thymic seeding, but is critical for the development of αβ T cell progenitors after seeding has occurred (Figures 2 and 3). In contrast, Rpl22l1 functions to promote the emergence of definitive HSC, which it supports by posttranscriptionally facilitating the expression of Smad1, a critical effector of the BMP4 signals upon which HSC emergence depends (Figures 6 and 7). The ability of Rpl22l1 to promote Smad1 expression and HSC emergence is directly opposed by Rpl22, which acts to repress Smad1 expression. Consequently, HSC emergence is critically regulated by the balance of Rpl22 and Rpl22l1, such that Rpl22l1 predominance promotes Smad1 expression and HSC emergence, while Rpl22 predominance represses them (Figure 7H).

While previous analysis in yeast and *Arabidopsis* suggests that some RP paralogs perform distinct functions (Degenhardt and Bonham-Smith, 2008; Komili et al., 2007; Steffen et al., 2008), ours is the first comparative analysis of RP paralog function in vertebrates. Two potential explanations have been advanced for the distinct phenotypes observed upon loss-of-function of RP paralogs. The first suggests that loss of RP paralogs causes distinct phenotypes by impairing ribosome biogenesis or translation to differing degrees, simply because processes differ in their sensitivity to reductions in protein synthesis (Komili et al., 2007; Lucioli et al., 1988). The alternative explanation is that some RP, and their paralogs, actually perform distinct functions either from within "specialized ribosomes" or in an "extraribosomal" capacity (Xue and Barna, 2012). Our findings support the latter interpretation, since Rpl22 and Rpl22l1 knockdown did not adversely affect protein synthesis (Figures S6D–S6F). More importantly, the rescue of HSC emergence in *rpl22/rpl22l1* double morphants cannot be explained by differential effects on protein synthesis. It remains unclear whether Rpl22 and Rpl22l1 exert their distinct effects on development from within specialized ribosomes or extraribosomally; however, the recent 80S ribosome crystal structure indicates that Rpl22 is not located near the sites of mRNA entry or peptide exit (Ben-Shem et al., 2011; Klinge et al., 2011). This, coupled with the ability of Rpl22 and Rpl22l1 to bind *smad1* mRNA, suggests that these RP may have functions outside of the ribosome.

Rpl22-deficiency blocks αβ T cell development in a p53-dependent manner (Figures 2 and 7H) (Anderson et al., 2007); however, the basis by which p53 induction is restricted to αβ T cell progenitors is unclear at present. Mutations in other RP have previously been linked to p53 induction through impaired ribosome biogenesis, which stabilizes p53 by blocking its degradation by MDM2 (Zhang and Lu, 2009). RP mutations that induce p53 in this manner cause widespread p53-induction, gross disruption of body morphology, and embryonic lethality in zebrafish (Chakraborty et al., 2009; Danilova et al., 2008). This seems an unlikely explanation for the induction of p53 upon Rpl22 knockdown, because p53 induction is restricted to αβ lineage thymocytes and is mediated by increased p53 translation (Anderson et al., 2007). Accordingly, we favor a model where Rpl22 acts extraribosomally to control p53 expression by either directly binding p53 mRNA or indirectly through controlling the expression of another regulator of p53 synthesis.

In contrast to Rpl22, Rpl22l1 plays an essential role in HSC emergence by facilitating Smad1 expression and consequently, the BMP4-mediated induction of Runx1 (Figures 5, 6, and 7). Runx1 expression in the VDA is also impaired in zebrafish bearing mutations in other RP or factors involved in ribosome biogenesis (*rps29*, *wdr43-like*, and *nop14-like*); however, these mutants exhibited gross morphologic abnormalities that were,

WISH at 24 hpf (*runx1)* and 36 hpf (*c-myb)* and the effect on thymus seeding was assessed at 5 dpf using the *Tg(ikaros:EGFP)* to mark thymic progenitors. VDA (F, red arrowheads); thymus (G, red circle).

(H) Model of Rpl22 and Rpl22l1 function in hematopoiesis. Our analysis indicates that Rpl22l1 promotes Runx1 induction and HSC emergence by facilitating Smad1 expression and BMP signaling. The promotion of Smad1 expression by Rpl22l1 is antagonized by Rpl22, perhaps through direct binding of *smad1* mRNA. In contrast, Rpl22 is dispensable for the emergence of HSC and consequent seeding of the thymus by progenitors; however, Rpl22 plays a critical role in supporting the development of thymic progenitors after seeding, by suppressing p53 expression in a lineage-restricted manner.

Images depict phenotypes representative of at least three separate experiments, with numbers referring to the fraction of morphants with the depicted phenotypes. See also Figure S6.

in the one case examined (*rps29*), attributable to p53 activation (Figures 4 and S3) (Burns et al., 2009; Taylor et al., 2012). The arrest of HSC emergence in *rpl22l1* morphants is not accompanied by gross morphological defects and is p53-independent, instead resulting from reduced Smad1 expression, which disrupts BMP/Smad signaling. Consistent with this interpretation, knockdown of Bmp4 and Smad1 causes a similar, selective impairment in development of definitive HSC (McReynolds et al., 2007; Wilkinson et al., 2009). While Smad1 is clearly an important target of the regulation of HSC emergence by Rpl22 and Rpl22l1, other targets may also play a role. Specifically, we have recently shown that Rpl22 loss in murine thymocytes and MEF increased the expression of the stemness factor Lin28B, whose enforced expression can replicate certain aspects of fetal lymphoid development (Rao et al., 2012; Yuan et al., 2012). Notably, there is no evidence that Lin28B plays a role in HSC emergence or is regulated by Rpl22/Rpl22l1 antagonism; however, efforts are nevertheless underway to address these possibilities.

The mechanism by which Rpl22l1 knockdown represses Smad1 protein levels remains incompletely understood; however, our data (Figures 6 and 7) suggest that Smad1 expression is regulated by the antagonistic balance of Rpl22l1 and Rpl22, such that when Rpl22l1 predominates, Smad1 expression is facilitated, whereas Rpl22 predominance results in Smad1 repression. Both Rpl22 and Rpl22l1 can bind *smad1* mRNA, suggesting that the opposing effects they have on Smad1 expression, result from binding *smad1* mRNA (Figures 6 and 7). Accordingly, the simplest mechanistic explanation for control of Smad1 expression by Rpl22 and Rpl22l1, is that both proteins bind *smad1* mRNA and induce the assembly of ribonucleoprotein complexes that either decrease or increase, respectively, translation of *smad1* mRNA. Several observations support this view. First, the ability of ectopically-expressed Rpl22 to repress Smad1 expression depends on its ability to bind RNA. Second, the representation of *smad1* mRNA in polysomes is reduced in *rpl22l1* morphants. Finally, Rpl22 is able to compete for Rpl22l1 binding to the 5′ UTR of *smad1* mRNA. Nevertheless, neither the sites in *smad1* mRNA bound by Rpl22 and Rpl22l1, nor the role of competition for binding in regulating Smad1 expression has been explored. Efforts to address these questions are currently underway.

How might homologous proteins like Rpl22 and Rpl22l1 exert opposing effects on targets? The RNA binding helices of Rpl22 and Rpl22l1 are identical, but these proteins are more divergent at their N and C termini (Figures 1 and S1). Accordingly, an attractive model is that these paralogs bind to a largely overlapping spectrum of RNA targets; however, they exert distinct effects on those targets, because their N/C-terminal sequences mediate interactions with a distinct set of cofactors. Specifically, Rpl22 might interact with cofactors that negatively regulate target expression, while Rpl22l1 interacts with distinct cofactors that oppose this action. Similar explanations have been advanced to suggest that the paralog of *RPS4*, *RPS4Y2*, might perform distinct functions (Lopes et al., 2010). Greater insight into the molecular basis for the distinct functions of Rpl22 and Rpl22l1 will require addressing the importance of the N and C termini and identifying their interacting partners.

Genomic analysis suggests that Rpl22 and Rpl22l1 might play important roles not only in normal stem cells but also in cancer. Rpl22 is enriched in mouse neuronal, embryonic, hematopoietic, and spermatogonial stem cell populations (Ramalho-Santos et al., 2002). Rpl22l1 is induced in HSC, perhaps by BMP signaling, as has been reported in ovarian germ stem cells in *Drosophila*, where its expression is inversely correlated with differentiation (Kai et al., 2005). The antagonistic relationship between Rpl22 and Rpl22l1 may play a critical role in modulating stem cell production, which if unchecked could lead to malignancy. Indeed, it is interesting that the *RPL22L1* gene resides in human 3q26 (Figure 1D), which is frequently amplified in a variety of human cancers, such as leukemia, ovarian, lung, head and neck, liver, and breast (Guan et al., 2004; Nanjundan et al., 2007; Shayesteh et al., 1999). Conversely, the locus encoding *RPL22* (1p36) is frequently deleted in cancer and contains many tumor suppressors, including *RPL22* (Figure 1C) (Bagchi et al., 2007; Rao et al., 2012). It is noteworthy that either *RPL22* inactivation or *RPL22L1* amplification would tip the balance in favor of Rpl22l1. Since both are associated with malignancy, careful control of antagonistic balance of Rpl22 and Rpl22l1 may be important not only for HSC emergence, but might also safeguard against malignancy.

Our data reveal critical, distinct, and antagonistic roles for the RP paralogs, Rpl22 and Rpl22l1, in regulating HSC emergence. Further studies are needed to gain insight into the molecular basis for their distinct functions and, importantly, whether they are exerted from within the ribosome or represent a growing list of RP that have been co-opted to function extraribosomally.

EXPERIMENTAL PROCEDURES

Zebrafish Maintenance and Lines

Zebrafish were housed at 28.5°C under standard aquaculture conditions. Animal housing and handling were all performed in accord with the approved protocol from the Institutional Animal Care and Use Committee. Embryos were staged as described previously (Kimmel et al., 1995). The AB wild-type, mutant, and lineage marking transgenic fish were used for MO, mRNA, and plasmid injections. The fish lines employed are listed in the Supplemental Experimental Procedures.

Bioinformatics

Genomic sequences were obtained by searching the UCSC and ENSEMBL databases. Multiple alignments of Rpl22 and Rpl22l1 amino acid sequences were obtained using Clustal W2 (http://www.ebi.ac.uk/Tools/clustalw2/index.html) and with the Neighbor Joining method to construct a phylogenetic tree using MEGA 4.0 software (Tamura et al., 2007). Synteny analysis of the zebrafish orthologs of *Rpl22* and *Rpl22l1* was performed as described previously (Liu et al., 2003).

Analysis of Zebrafish Morphants

Antisense MO oligonucleotides (Gene Tools, LLC) were injected into 1- or 2-cell stage zebrafish embryos at the indicated concentrations. MO sequences are listed in Supplemental Experimental Procedures.

WISH Analysis and Apoptosis Assay

WISH and whole-mount TUNEL assays were carried out as described (Bennett et al., 2001; Liu et al., 2003). The stained embryos were mounted in 2% methylcellulose and photographed using the Nikon SMZ1500 stereomicroscope equipped with DS-Fi1 digital camera and Nikon Ar imaging software.

Plasmid Constructs, RNA Production, and Transient Overexpression Studies

RNAs injected into zebrafish embryos were produced by in vitro transcription. Heat shock-inducible expression of mouse Rpl22 and Rpl22l1 was accomplished using the heat-inducible pSGH2 vector and heating to 37°C for 1 hr as described (Bajoghli et al., 2004). See Supplemental Experimental Procedures for details.

Protein Expression and Purification

Recombinant proteins were produced in *Escherichia coli* as either GST or His-tagged fusions and purified using glutathione- or nickel-Sepharose, respectively using standard methods. See Supplemental Experimental Proceduresfor details.

RNA Binding Assays

To assess RNA binding by Rpl22 and Rpl22l1, the indicated RNA targets were synthesized by in vitro transcription and incubated with recombinant fusion proteins, after which RNA binding was assessed by RPA. RNA binding was also evaluated by EMSA in which detergent extracts from Rpl22−/− MEF were supplemented with in vitro transcribed RNA targets and Rpl22 or Rpl22l1 fusion proteins. Band shifts were evaluated by nondenaturing gel electrophoresis. See Supplemental ExperimentalProcedures for details.

Real-Time PCR, Protein Extraction, and Western Blotting

Total RNA from pools of embryos was extracted using Trizol according to manufacturer's suggestions and reverse transcribed, after which RNA targets were quantified using TaqMan real-time PCR primer/probes (listed in Supplemental Experimental Procedures). The relative expression values were normalized to *gapdh*. Protein extraction and western blotting were carried out as described, with antibodies listed in Supplemental Experimental Procedures (Link et al., 2006).

Fluorescence-Activated Cell Sorting

Transgenic embryos were dissected with trypsin/EDTA (Life Technologies), after which a single-cell suspension was produced by passage through a 40-μm nylon mesh, prior to flow cytometric isolation using the FACSVantageSE (Becton Dickinson Immunocytometry Systems, San Jose, CA).

Polysome Isolation and Real-Time PCR Quantification of *smad1* mRNA

Detergent extracts of embryos were layered over a 17%–50% sucrose gradient, after which polysomes were resolved by centrifugation at 37,000 × g for 2 hr at 4°C. Gradient samples were harvested and RNA content was monitored using a UV flow cell at $O.D._{254}$. *smad1* mRNA content of the gradient fractions was quantified by real-time PCR and normalized to β-actin. See Supplemental Experimental Procedures for details.

Statistical Analysis

A Student's t test was used in the experiments shown in Figure 3. Statistical significance was accepted when $p < 0.05$.

SUPPLEMENTAL INFORMATION

Supplemental Information includes six figures and Supplemental Experimental Procedures and can be found with this article online at http://dx.doi.org/10.1016/j.devcel.2013.01.018.

ACKNOWLEDGMENTS

We thank Drs. Dietmar Kappes, Brian Kennedy, Dmitri Pestov, Jackie Perrigoue, Jason Stadanlick, Randy Strich, Nikolaus Trede, and Alexei Tulin for critical comments on the manuscript, Dr. Thomas Boehm for providing the *Tg(ikaros:EGFP)* transgenic line, *tcrb2*, and *tcrd* probes, Drs. Trede, Roger Patient, Mary Mullins, Matthias Hammerschmidt, Pengfei Xu, Hao Yuan, and Jun Zhu, for providing *lck*, *c-myb*, *bmp4*, *smad1*, *smad5* probes, full-length cDNA, and pSGH2 vector, and Sang-Yun Lee, Darius Balciunas, Francis Coffey, Megan Fisher, Xingjun Liu, Qin Li, Mara Robu, Madhusmita Datta, Suzanne McDaniels, George Merkel, Jinhua Wu, and Bruce Young for technical assistance with the project. Finally, we gratefully acknowledge the assistance of the following core facilities of the Fox Chase Cancer Center: Flow Cytometry, DNA Sequencing, Imaging and Laboratory Animal/Zebrafish. This work was supported by NIH grants AI081814, AI073920, NIH core grant P01CA06927, Center grant P30-DK-50306, and an appropriation from the Commonwealth of Pennsylvania.

Received: April 22, 2011
Revised: November 15, 2012
Accepted: January 20, 2013
Published: February 25, 2013

REFERENCES

Amsterdam, A., Sadler, K.C., Lai, K., Farrington, S., Bronson, R.T., Lees, J.A., and Hopkins, N. (2004). Many ribosomal protein genes are cancer genes in zebrafish. PLoS Biol. *2*, E139.

Anderson, S.J., Lauritsen, J.P., Hartman, M.G., Foushee, A.M., Lefebvre, J.M., Shinton, S.A., Gerhardt, B., Hardy, R.R., Oravecz, T., and Wiest, D.L. (2007). Ablation of ribosomal protein L22 selectively impairs alphabeta T cell development by activation of a p53-dependent checkpoint. Immunity *26*, 759–772.

Bagchi, A., Papazoglu, C., Wu, Y., Capurso, D., Brodt, M., Francis, D., Bredel, M., Vogel, H., and Mills, A.A. (2007). CHD5 is a tumor suppressor at human 1p36. Cell *128*, 459–475.

Bajoghli, B., Aghaallaei, N., Heimbucher, T., and Czerny, T. (2004). An artificial promoter construct for heat-inducible misexpression during fish embryogenesis. Dev. Biol. *271*, 416–430.

Ben-Shem, A., Garreau de Loubresse, N., Melnikov, S., Jenner, L., Yusupova, G., and Yusupov, M. (2011). The structure of the eukaryotic ribosome at 3.0 Å resolution. Science *334*, 1524–1529.

Bennett, C.M., Kanki, J.P., Rhodes, J., Liu, T.X., Paw, B.H., Kieran, M.W., Langenau, D.M., Delahaye-Brown, A., Zon, L.I., Fleming, M.D., and Look, A.T. (2001). Myelopoiesis in the zebrafish, Danio rerio. Blood *98*, 643–651.

Bertrand, J.Y., Kim, A.D., Teng, S., and Traver, D. (2008). CD41+ cmyb+ precursors colonize the zebrafish pronephros by a novel migration route to initiate adult hematopoiesis. Development *135*, 1853–1862.

Bertrand, J.Y., Chi, N.C., Santoso, B., Teng, S., Stainier, D.Y., and Traver, D. (2010). Haematopoietic stem cells derive directly from aortic endothelium during development. Nature *464*, 108–111.

Boehm, T., and Bleul, C.C. (2006). Thymus-homing precursors and the thymic microenvironment. Trends Immunol. *27*, 477–484.

Boisset, J.C., van Cappellen, W., Andrieu-Soler, C., Galjart, N., Dzierzak, E., and Robin, C. (2010). In vivo imaging of haematopoietic cells emerging from the mouse aortic endothelium. Nature *464*, 116–120.

Burns, C.E., Galloway, J.L., Smith, A.C., Keefe, M.D., Cashman, T.J., Paik, E.J., Mayhall, E.A., Amsterdam, A.H., and Zon, L.I. (2009). A genetic screen in zebrafish defines a hierarchical network of pathways required for hematopoietic stem cell emergence. Blood *113*, 5776–5782.

Chakraborty, A., Uechi, T., Higa, S., Torihara, H., and Kenmochi, N. (2009). Loss of ribosomal protein L11 affects zebrafish embryonic development through a p53-dependent apoptotic response. PLoS ONE *4*, e4152.

Chen, M.J., Yokomizo, T., Zeigler, B.M., Dzierzak, E., and Speck, N.A. (2009). Runx1 is required for the endothelial to haematopoietic cell transition but not thereafter. Nature *457*, 887–891.

Danilova, N., Sakamoto, K.M., and Lin, S. (2008). Ribosomal protein S19 deficiency in zebrafish leads to developmental abnormalities and defective erythropoiesis through activation of p53 protein family. Blood *112*, 5228–5237.

Degenhardt, R.F., and Bonham-Smith, P.C. (2008). Arabidopsis ribosomal proteins RPL23aA and RPL23aB are differentially targeted to the nucleolus and are disparately required for normal development. Plant Physiol. *147*, 128–142.

Deisenroth, C., and Zhang, Y. (2010). Ribosome biogenesis surveillance: probing the ribosomal protein-Mdm2-p53 pathway. Oncogene *29*, 4253–4260.

Dobbelstein, M., and Shenk, T. (1995). In vitro selection of RNA ligands for the ribosomal L22 protein associated with Epstein-Barr virus-expressed RNA by using randomized and cDNA-derived RNA libraries. J. Virol. *69*, 8027–8034.

Draptchinskaia, N., Gustavsson, P., Andersson, B., Pettersson, M., Willig, T.N., Dianzani, I., Ball, S., Tchernia, G., Klar, J., Matsson, H., et al. (1999). The gene encoding ribosomal protein S19 is mutated in Diamond-Blackfan anaemia. Nat. Genet. *21*, 169–175.

Ebert, B.L., Pretz, J., Bosco, J., Chang, C.Y., Tamayo, P., Galili, N., Raza, A., Root, D.E., Attar, E., Ellis, S.R., and Golub, T.R. (2008). Identification of RPS14 as a 5q- syndrome gene by RNA interference screen. Nature *451*, 335–339.

Georgopoulos, K., Winandy, S., and Avitahl, N. (1997). The role of the Ikaros gene in lymphocyte development and homeostasis. Annu. Rev. Immunol. *15*, 155–176.

Goessling, W., North, T.E., and Zon, L.I. (2007). New waves of discovery: modeling cancer in zebrafish. J. Clin. Oncol. *25*, 2473–2479.

Guan, X.Y., Fung, J.M., Ma, N.F., Lau, S.H., Tai, L.S., Xie, D., Zhang, Y., Hu, L., Wu, Q.L., Fang, Y., and Sham, J.S. (2004). Oncogenic role of eIF-5A2 in the development of ovarian cancer. Cancer Res. *64*, 4197–4200.

Haarer, B., Viggiano, S., Hibbs, M.A., Troyanskaya, O.G., and Amberg, D.C. (2007). Modeling complex genetic interactions in a simple eukaryotic genome: actin displays a rich spectrum of complex haploinsufficiencies. Genes Dev. *21*, 148–159.

Houmani, J.L., Davis, C.I., and Ruf, I.K. (2009). Growth-promoting properties of Epstein-Barr virus EBER-1 RNA correlate with ribosomal protein L22 binding. J. Virol. *83*, 9844–9853.

Jin, H., Xu, J., and Wen, Z. (2007). Migratory path of definitive hematopoietic stem/progenitor cells during zebrafish development. Blood *109*, 5208–5214.

Kai, T., Williams, D., and Spradling, A.C. (2005). The expression profile of purified Drosophila germline stem cells. Dev. Biol. *283*, 486–502.

Kimmel, C.B., Ballard, W.W., Kimmel, S.R., Ullmann, B., and Schilling, T.F. (1995). Stages of embryonic development of the zebrafish. Dev. Dyn. *203*, 253–310.

Kissa, K., and Herbomel, P. (2010). Blood stem cells emerge from aortic endothelium by a novel type of cell transition. Nature *464*, 112–115.

Kissa, K., Murayama, E., Zapata, A., Cortés, A., Perret, E., Machu, C., and Herbomel, P. (2008). Live imaging of emerging hematopoietic stem cells and early thymus colonization. Blood *111*, 1147–1156.

Klinge, S., Voigts-Hoffmann, F., Leibundgut, M., Arpagaus, S., and Ban, N. (2011). Crystal structure of the eukaryotic 60S ribosomal subunit in complex with initiation factor 6. Science *334*, 941–948.

Komili, S., Farny, N.G., Roth, F.P., and Silver, P.A. (2007). Functional specificity among ribosomal proteins regulates gene expression. Cell *131*, 557–571.

Kondrashov, N., Pusic, A., Stumpf, C.R., Shimizu, K., Hsieh, A.C., Xue, S., Ishijima, J., Shiroishi, T., and Barna, M. (2011). Ribosome-mediated specificity in Hox mRNA translation and vertebrate tissue patterning. Cell *145*, 383–397.

Lam, E.Y., Chau, J.Y., Kalev-Zylinska, M.L., Fountaine, T.M., Mead, R.S., Hall, C.J., Crosier, P.S., Crosier, K.E., and Flores, M.V. (2009). Zebrafish runx1 promoter-EGFP transgenics mark discrete sites of definitive blood progenitors. Blood *113*, 1241–1249.

Lam, E.Y., Hall, C.J., Crosier, P.S., Crosier, K.E., and Flores, M.V. (2010). Live imaging of Runx1 expression in the dorsal aorta tracks the emergence of blood progenitors from endothelial cells. Blood *116*, 909–914.

Langenau, D.M., Ferrando, A.A., Traver, D., Kutok, J.L., Hezel, J.P., Kanki, J.P., Zon, L.I., Look, A.T., and Trede, N.S. (2004). In vivo tracking of T cell development, ablation, and engraftment in transgenic zebrafish. Proc. Natl. Acad. Sci. USA *101*, 7369–7374.

Lee, S.Y., Stadanlick, J., Kappes, D.J., and Wiest, D.L. (2010). Towards a molecular understanding of the differential signals regulating alphabeta/gammadelta T lineage choice. Semin. Immunol. *22*, 237–246.

Lieschke, G.J., and Trede, N.S. (2009). Fish immunology. Curr. Biol. *19*, R678–R682.

Link, V., Shevchenko, A., and Heisenberg, C.P. (2006). Proteomics of early zebrafish embryos. BMC Dev. Biol. *6*, 1.

Liu, T.X., Howlett, N.G., Deng, M., Langenau, D.M., Hsu, K., Rhodes, J., Kanki, J.P., D'Andrea, A.D., and Look, A.T. (2003). Knockdown of zebrafish Fancd2 causes developmental abnormalities via p53-dependent apoptosis. Dev. Cell *5*, 903–914.

Lopes, A.M., Miguel, R.N., Sargent, C.A., Ellis, P.J., Amorim, A., and Affara, N.A. (2010). The human RPS4 paralogue on Yq11.223 encodes a structurally conserved ribosomal protein and is preferentially expressed during spermatogenesis. BMC Mol. Biol. *11*, 33.

Lucioli, A., Presutti, C., Ciafrè, S., Caffarelli, E., Fragapane, P., and Bozzoni, I. (1988). Gene dosage alteration of L2 ribosomal protein genes in Saccharomyces cerevisiae: effects on ribosome synthesis. Mol. Cell. Biol. *8*, 4792–4798.

McReynolds, L.J., Gupta, S., Figueroa, M.E., Mullins, M.C., and Evans, T. (2007). Smad1 and Smad5 differentially regulate embryonic hematopoiesis. Blood *110*, 3881–3890.

Mukhopadhyay, R., Ray, P.S., Arif, A., Brady, A.K., Kinter, M., and Fox, P.L. (2008). DAPK-ZIPK-L13a axis constitutes a negative-feedback module regulating inflammatory gene expression. Mol. Cell *32*, 371–382.

Murayama, E., Kissa, K., Zapata, A., Mordelet, E., Briolat, V., Lin, H.F., Handin, R.I., and Herbomel, P. (2006). Tracing hematopoietic precursor migration to successive hematopoietic organs during zebrafish development. Immunity *25*, 963–975.

Nanjundan, M., Nakayama, Y., Cheng, K.W., Lahad, J., Liu, J., Lu, K., Kuo, W.L., Smith-McCune, K., Fishman, D., Gray, J.W., and Mills, G.B. (2007). Amplification of MDS1/EVI1 and EVI1, located in the 3q26.2 amplicon, is associated with favorable patient prognosis in ovarian cancer. Cancer Res. *67*, 3074–3084.

Narla, A., and Ebert, B.L. (2010). Ribosomopathies: human disorders of ribosome dysfunction. Blood *115*, 3196–3205.

Pestov, D.G., Strezoska, Z., and Lau, L.F. (2001). Evidence of p53-dependent cross-talk between ribosome biogenesis and the cell cycle: effects of nucleolar protein Bop1 on G(1)/S transition. Mol. Cell. Biol. *21*, 4246–4255.

Pimanda, J.E., Donaldson, I.J., de Bruijn, M.F., Kinston, S., Knezevic, K., Huckle, L., Piltz, S., Landry, J.R., Green, A.R., Tannahill, D., and Göttgens, B. (2007). The SCL transcriptional network and BMP signaling pathway interact to regulate RUNX1 activity. Proc. Natl. Acad. Sci. USA *104*, 840–845.

Ramalho-Santos, M., Yoon, S., Matsuzaki, Y., Mulligan, R.C., and Melton, D.A. (2002). "Stemness": transcriptional profiling of embryonic and adult stem cells. Science *298*, 597–600.

Rao, S., Lee, S.Y., Gutierrez, A., Perrigoue, J., Thapa, R.J., Tu, Z., Jeffers, J.R., Rhodes, M., Anderson, S., Oravecz, T., et al. (2012). Inactivation of ribosomal protein L22 promotes transformation by induction of the stemness factor, Lin28B. Blood *120*, 3764–3773.

Rotenberg, M.O., Moritz, M., and Woolford, J.L., Jr. (1988). Depletion of Saccharomyces cerevisiae ribosomal protein L16 causes a decrease in 60S ribosomal subunits and formation of half-mer polyribosomes. Genes Dev. *2*, 160–172.

Shayesteh, L., Lu, Y., Kuo, W.L., Baldocchi, R., Godfrey, T., Collins, C., Pinkel, D., Powell, B., Mills, G.B., and Gray, J.W. (1999). PIK3CA is implicated as an oncogene in ovarian cancer. Nat. Genet. *21*, 99–102.

Sonenberg, N., and Hinnebusch, A.G. (2009). Regulation of translation initiation in eukaryotes: mechanisms and biological targets. Cell *136*, 731–745.

Steffen, K.K., MacKay, V.L., Kerr, E.O., Tsuchiya, M., Hu, D., Fox, L.A., Dang, N., Johnston, E.D., Oakes, J.A., Tchao, B.N., et al. (2008). Yeast life span extension by depletion of 60s ribosomal subunits is mediated by Gcn4. Cell *133*, 292–302.

Su, D.M., Navarre, S., Oh, W.J., Condie, B.G., and Manley, N.R. (2003). A domain of Foxn1 required for crosstalk-dependent thymic epithelial cell differentiation. Nat. Immunol. *4*, 1128–1135.

Tamura, K., Dudley, J., Nei, M., and Kumar, S. (2007). MEGA4: Molecular Evolutionary Genetics Analysis (MEGA) software version 4.0. Mol. Biol. Evol. *24*, 1596–1599.

Taylor, A.M., Humphries, J.M., White, R.M., Murphey, R.D., Burns, C.E., and Zon, L.I. (2012). Hematopoietic defects in rps29 mutant zebrafish depend upon p53 activation. Exp. Hematol. *40*, 228–237.

Tucker, J.A., Mintzer, K.A., and Mullins, M.C. (2008). The BMP signaling gradient patterns dorsoventral tissues in a temporally progressive manner along the anteroposterior axis. Dev. Cell *14*, 108–119.

Warner, J.R., and McIntosh, K.B. (2009). How common are extraribosomal functions of ribosomal proteins? Mol. Cell *34*, 3–11.

Wilkinson, R.N., Pouget, C., Gering, M., Russell, A.J., Davies, S.G., Kimelman, D., and Patient, R. (2009). Hedgehog and Bmp polarize hematopoietic stem cell emergence in the zebrafish dorsal aorta. Dev. Cell *16*, 909–916.

Xue, S., and Barna, M. (2012). Specialized ribosomes: a new frontier in gene regulation and organismal biology. Nat. Rev. Mol. Cell Biol. *13*, 355–369.

Yuan, J., Nguyen, C.K., Liu, X., Kanellopoulou, C., and Muljo, S.A. (2012). Lin28b reprograms adult bone marrow hematopoietic progenitors to mediate fetal-like lymphopoiesis. Science *335*, 1195–1200.

Zhang, Y., and Lu, H. (2009). Signaling to p53: ribosomal proteins find their way. Cancer Cell *16*, 369–377.